doi:10.1093/brain/awt088 Brain 2013: 136; 1913–1928 | 1913

BRAIN
A JOURNAL OF NEUROLOGY

The influence of phospho-tau on dendritic spines of cortical pyramidal neurons in patients with Alzheimer's disease

Paula Merino-Serrais,[1,2,3] Ruth Benavides-Piccione,[1,2,3] Lidia Blazquez-Llorca,[1,2,3] Asta Kastanauskaite,[1,2,3] Alberto Rábano,[4] Jesús Avila[3,5] and Javier DeFelipe[1,2,3]

1 Laboratorio Cajal de Circuitos Corticales (CTB), Universidad Politécnica de Madrid, Campus Montegancedo S/N, 28223 Pozuelo de Alarcón, Spain
2 Instituto Cajal (CSIC), Avda Doctor Arce 37, 28002 Madrid, Spain
3 Centro de Investigación Biomédica en Red sobre Enfermedades Neurodegenerativas (CIBERNED), Spain
4 Departamento de Neuropatología y Banco de Tejidos, Fundación CIEN, C/ Valderrebollo 5, 28031 Madrid, Spain
5 Centro de Biología Molecular 'Severo Ochoa' (CSIC-UAM), C/ Nicolás Cabrera 1, Campus de Cantoblanco, Universidad Autónoma de Madrid, 28049 Madrid, Spain

Correspondence to: Javier DeFelipe,
Laboratorio Cajal de Circuitos Corticales,
Centro de Tecnología Biomédica,
Universidad Politécnica de Madrid,
Campus Montegancedo S/N,
Pozuelo de Alarcón,
28223 Madrid; or Instituto Cajal (CSIC),
Avenida Doctor Arce 37,
28002 Madrid,
Spain
E-mail: defelipe@cajal.csic.es

The dendritic spines on pyramidal cells represent the main postsynaptic elements of cortical excitatory synapses and they are fundamental structures in memory, learning and cognition. In the present study, we used intracellular injections of Lucifer yellow in fixed tissue to analyse over 19 500 dendritic spines that were completely reconstructed in three dimensions along the length of the basal dendrites of pyramidal neurons in the parahippocampal cortex and CA1 of patients with Alzheimer's disease. Following intracellular injection, sections were immunostained for anti-Lucifer yellow and with tau monoclonal antibodies AT8 and PHF-1, which recognize tau phosphorylated at Ser202/Thr205 and at Ser396/404, respectively. We observed that the diffuse accumulation of phospho-tau in a putative pre-tangle state did not induce changes in the dendrites of pyramidal neurons, whereas the presence of tau aggregates forming intraneuronal neurofibrillary tangles was associated with progressive alteration of dendritic spines (loss of dendritic spines and changes in their morphology) and dendrite atrophy, depending on the degree of tangle development. Thus, the presence of phospho-tau in neurons does not necessarily mean that they suffer severe and irreversible effects as thought previously but rather, the characteristic cognitive impairment in Alzheimer's disease is likely to depend on the relative number of neurons that have well developed tangles.

Keywords: intracellular injection; hippocampal formation; dendritic spine density and volume; 3D reconstruction; confocal microscopy

Abbreviations: ir = immunoreactive; PHF = paired helical filaments

Received August 23, 2012. Revised February 8, 2013. Accepted February 17, 2013

Introduction

In the brain, abnormal phosphorylation of the microtubule-associated protein tau leads to the formation of paired helical filaments (PHFs), the main components of intraneuronal neurofibrillary tangles (Grundke-Iqbal *et al*., 1986). These alterations, along with the appearance of extracellular fibrillar amyloid-β peptide in plaques, are the main histopathological hallmarks of Alzheimer's disease. However, there is only a weak correlation between the degree of cognitive impairment and the presence of plaques or neurofibrillary tangles (Price *et al*., 2009) and thus, it is necessary for us to better understand this association.

At present there is considerable interest in examining the possible alterations to pyramidal cells associated with brain disease, and their role in memory, learning and cognition (Fiala *et al*., 2002; Benavides-Piccione *et al*., 2004; Spruston, 2008; Luebke *et al*., 2010; Penzes *et al*., 2011). Pyramidal cells are the most abundant neurons in the cortex (estimated to represent 70–80% of the total neuronal population), where they are the main source of excitatory (glutamatergic) synapses. The dendritic spines on pyramidal cells are the main postsynaptic target of excitatory synapses in the cerebral cortex and thus, pyramidal cells are considered the principal building blocks of this structure (DeFelipe and Fariñas, 1992). For example, changes in the number of dendritic spines are indicative of the differences in the number of excitatory inputs that pyramidal cells receive, whereas the spine head volume is correlated with the area of the postsynaptic density. In turn, the size of the postsynaptic density is correlated with the number of presynaptic vesicles, the number of postsynaptic receptors and the ready-releasable pool of transmitter (Harris and Stevens, 1989; Nusser *et al*., 1998; Schikorski and Stevens, 1999, 2001; Arellano *et al*., 2007*a*). Moreover, the length of the spine neck is proportional to the extent of biochemical and electrical isolation of the spine from its parent dendrite (Majewska *et al*., 2000*a*, *b*; Araya *et al*., 2006). As a consequence, analysing the microanatomy of dendritic spines of pyramidal cells represents an excellent opportunity to study the structural substrate of cognitive impairment in Alzheimer's disease.

Previous studies in animal models of Alzheimer's disease have shown that amyloid-β plaques induce local morphological alterations to the dendrites in contact with amyloid-β (Tsai *et al*., 2004; Spires *et al*., 2005; Knafo *et al*., 2009*a*, *b*; Merino-Serrais *et al*., 2011). Significantly, the expression of mutant tau in mouse models of Alzheimer's disease-like tau neuropathologies can result in a significant loss of dendritic spines and synapses (Mocanu *et al*., 2008; Bittner *et al*., 2010; Rocher *et al*., 2010). Therefore, the presence of PHF-tau is likely to be involved in the changes to dendritic spines and the loss of synapses that leads to cognitive decline in Alzheimer's disease. Unfortunately, this hypothesis has yet to be verified in patients with Alzheimer's disease due to the obvious ethical issues and the technical difficulties. Thus, the main aim of this study was to examine human cortical pyramidal cells with either diffuse phospho-tau in a putative pre-tangle state or aggregated tau that forms neurofibrillary tangles, as well as to assess the possible alterations to their dendritic spines, using intracellular injections of Lucifer yellow in fixed cortical tissue.

Materials and methods

Human brain tissue ($n = 5$) was obtained at autopsy from the 'Instituto de Neuropatología' (Dr I. Ferrer, Servicio de Anatomía Patológica, IDIBELL-Hospital Universitario de Bellvitge, Barcelona, Spain), from the 'Banco de Tejidos Fundación CIEN' (Centro Alzheimer, Fundación Reina Sofía, Madrid, Spain) and from the Neurological Tissue Bank (Biobanc-Hospital Clínic-IDIBAPS, Universidad de Barcelona, Spain). Following neuropathological examination, the pathological state and stage was defined according to the CERAD (Consortium to Establish a Registry for Alzheimer's Disease) (Mirra *et al*., 1991) and the Braak and Braak criteria (Braak and Braak, 1991; Supplementary Table 1). In all cases, the time between death and tissue fixation was 2–3 h, and the brain samples were obtained following the guidelines and with the approval of the Institutional Ethical Committee. The tissue from some of these human brains (Patients P9, P11, P12, P13 and P14) has been used in previous studies (Blazquez-Llorca *et al*., 2010, 2011).

Upon removal, the brain was immediately fixed in cold 4% paraformaldehyde in phosphate buffer (0.1 M, pH 7.4) and subsequently, small blocks of the hippocampal formation and adjacent cortex were obtained (10 × 10 × 10 mm) and post-fixed in the same fixative solution for 24 h at 4°C. After fixation, vibratome sections of the cortical tissue were obtained and intracellular injections, immunohistochemistry and histochemistry were performed (Supplementary material). The sections immediately adjacent were Nissl-stained (50 μm) in order to identify the cortical areas and the laminar boundaries. Briefly, individual pyramidal cells in the hippocampal formation and adjacent cortex were injected intracellularly with Lucifer yellow (Supplementary material). Following intracellular injection, sections were double immunostained with anti-Lucifer yellow and either anti-PHF-tau$_{AT8}$ or anti-PHF-tau$_{PHF\text{-}1}$ antibodies (Supplementary material). We then measured the diameter of the dendrites, dendritic spine density, as well as the dendritic spine length and volume of dendritic spines scanned by confocal microscopy and completely reconstructed in three dimensions using a methodology previously described in detail (Benavides-Piccione *et al*., 2012).

Statistics

For all the morphological parameters measured, the values were averaged per dendrite to give a mean per group. In addition, the data are presented as frequency distributions. To test the overall effect, a Mann-Whitney test was used to compare the averages (mean ± SEM) and the Kolmogorov-Smirnov test was used in the case of the frequencies. Two-way ANOVA followed by a *post hoc* multiple Bonferroni comparison was used to compare values when presented as a function of the distance from soma.

Results

Intracellular injections

A total of 704 cells in different cortical regions of the tissue from five patients were injected with Lucifer yellow (Supplementary Table 1). Although Lucifer yellow injected neurons were immunostained for either PHF-tau$_{AT8}$ or PHF-tau$_{PHF\text{-}1}$, we obtained sufficient labelled PHF-tau$_{AT8}$ positive neurons from only three patients ($n = 150$, 186 and 132 from Patients P9, P13 and P14, respectively) to perform a quantitative study on the possible differences

between neurons free of neurofibrillar pathology and those showing either diffuse phospho-tau in a putative pre-tangle state or tau aggregation forming neurofibrillary tangles. The selected pyramidal neurons for morphometric analysis of their basal dendrites were located in layer III of the parahippocampal cortex from Patient P9 and in the pyramidal cell layer of the CA1 from Patients P9, P13 and P14 (Fig. 1A). The remaining Lucifer yellow-injected neurons were used for qualitative analyses alone and as such, we shall concentrate on the more detailed neuropathological characteristics and morphometry of the tissue from Patients P9, P13 and P14, unless otherwise specified.

Neuropathological characteristics of the injected tissue

In sections from the hippocampal formation and adjacent cortex, numerous amyloid-β plaques, and PHF-tau$_{AT8}$-ir (immunoreactive) and PHF-tau$_{PHF-1}$-ir neurons were present, although the density and distribution of these labelled elements varied depending on the cortical region (Figs 1 and 2; Supplementary Figs 1 and 2).

Percentage of paired helical filament-tau immunoreactive neurons

Unbiased stereology was used to quantify the total density of neurons, and the density of PHF-tau$_{AT8}$-ir and PHF-tau$_{PHF-1}$-ir neurons in layer III of the parahippocampal cortex from Patient P9 and in the CA1 pyramidal cell layer of Patients P9, P13 and P14 (Supplementary Fig. 2). In Patient P9, the total neuron density in the parahippocampal cortex was 19 560 neurons/mm^3, whereas the density of PHF-tau$_{AT8}$-ir and PHF-tau$_{PHF-1}$-ir neurons was 2917 and 499 neurons/mm^3, respectively (Fig. 2), 15% and 2.5% of the total neuronal density, respectively. In the CA1 region, the total neuron density was 15 786 in Patient P9, 11 916 in Patient P13 and 12 193 in Patient P14 (neurons/mm^3), and the percentage of phospho-tau neurons varied between these patients (Fig. 2 and Supplementary material). The phospho-tau neurofibrillar pathology was stronger in the CA1 than in the parahippocampal cortex from Patient P9 (Fig. 2). Moreover, when comparing the total neuronal density with the density of PHF-tau$_{AT8}$-ir and PHF-tau$_{PHF-1}$-ir neurons, and the density of amyloid-β plaques, in the CA1 region of all three patients, it seems clear that the neuropathological alterations were greater in Patient P14, followed by Patient P13 and then Patient P9.

Patterns of paired helical filament tau staining

We previously established two patterns of immunostaining for PHF-tau$_{AT8}$-ir neurons according to the presence or absence of neurofibrillary tangles in the soma (Blazquez-Llorca *et al.*, 2010): Pattern I and Pattern II. Neurons with Pattern I have diffuse cytoplasmic staining, independent of the presence of some small fibrillar aggregates (putative pre-tangle stage) that may be thioflavin S positive. Neurons with Pattern II typically form neurofibrillary tangles (tangle stage). In the present study, we further subdivided Pattern II into Patterns IIa and IIb, depending on the extent of neurofibrillary tangle development visualized with PHF-tau$_{AT8}$, PHF-tau$_{PHF-1}$ and thioflavin S (Pattern IIa, intermediate/advanced stages; Pattern IIb, extreme stage: Fig. 3).

Morphometric analysis of Lucifer yellow-injected neurons

As a first step, Lucifer yellow-injected neurons selected for detailed quantitative studies were divided into PHF-tau$_{AT8}$-ir neurons and neurons that were non-immunostained for PHF-tau$_{AT8}$ (Figs 4 and 5; Supplementary Fig. 3) whose dendrites were not in contact with amyloid-β plaques (Supplementary Fig. 4). Because the density and pattern of immunostaining for PHF-tau$_{AT8}$ and PHF-tau$_{PHF-1}$ were similar but not identical (Supplementary Figs 1 and 2), it was possible that neurons that were non-immunostained for PHF-tau$_{AT8}$ were PHF-tau$_{PHF-1}$. Therefore, the next step was to check for the presence of PHF-tau$_{PHF-1}$ in Lucifer yellow-injected neurons that were non-immunostained for PHF-tau$_{AT8}$. To this end, sections were recovered and reprocessed immunocytochemically using anti-PHF-tau$_{PHF-1}$. All Lucifer yellow-injected neurons that were PHF-tau$_{AT8}$-ir were also PHF-tau$_{PHF-1}$, whereas some Lucifer yellow-injected neurons that were non-immunostained for PHF-tau$_{AT8}$ were also labelled for PHF-tau$_{PHF-1}$ (Supplementary Fig. 5). Therefore, we established two groups of Lucifer yellow-injected neurons for quantitative studies: neurons that were immunostained for both PHF-tau$_{AT8}$ and PHF-tau$_{PHF-1}$ and neurons that were not immunostained by either of the two antibodies. For the sake of simplicity and unless otherwise specified, we called these Lucifer yellow-injected neurons PHF-tau$^+$ and PHF-tau$^-$ neurons, respectively. Nevertheless, it is important to mention that both PHF-tau$_{AT8}$ and PHF-tau$_{PHF-1}$ antibodies were produced in mouse. Thus, the labeling of neurons for both PHF-tau$_{AT8}$ PHF-tau$_{PHF-1}$ could be due to antibody cross-reactivity.

In the present study, a total of 42 Lucifer yellow-injected neurons and 19 569 dendritic spines were examined in three dimensions (10 334 dendritic spines from PHF-tau$^-$ neurons and 9235 from PHF-tau$^+$ neurons whose dendrites are not in contact with amyloid-β plaques; Supplementary Fig. 4). In the parahippocampal cortex from Patient P9, all the Lucifer yellow-injected neurons analysed that were PHF-tau$^+$ were considered to be Pattern I, whereas in the CA1 from Patients P9, P13 and P14, all the Lucifer yellow-injected neurons analysed that were PHF-tau$^+$ were Pattern IIa. Unexpectedly, it initially appeared that the microanatomical characteristics of the dendrites from the Lucifer yellow-injected neurons that were PHF-tau$^-$ were apparently similar to those whose soma was PHF-tau$^+$, showing either Pattern I (Fig. 4) or Pattern IIa (Fig. 5).

However, when PHF-tau$^+$ neurons that had well developed neurofibrillary tangles (Pattern IIb) were injected, these neurons had a reduced dendritic arbor and few or virtually no dendritic spines. The dendritic diameter was also remarkably thin in all these cases (Fig. 6). These neurons were not further analysed.

As a result of these findings, a quantitative analysis of the morphological parameters was performed that included the dendrite diameter, dendritic spine density, length and volume of dendritic

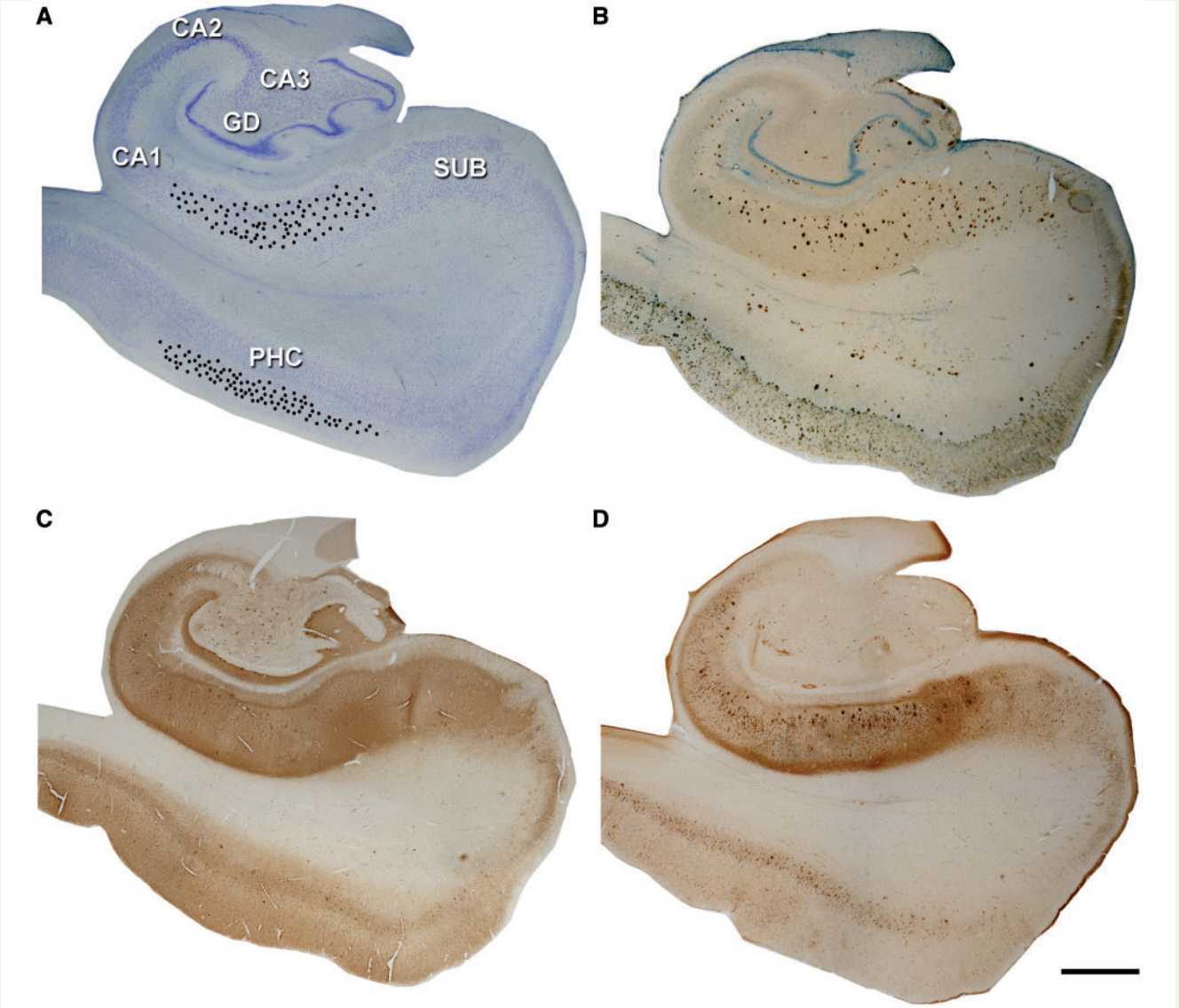

Figure 1 Localization of intracellular injections and histopathology. Low-power photomicrographs of Nissl (**A**), amyloid-β/Nissl (**B**), PHF-tau$_{AT8}$ (**C**) and PHF-tau$_{PHF-1}$ (**D**) stained sections from Patient P9. The black dots in (**A**) show the approximate location of the injected neurons in layer III of the parahippocampal cortex (PHC) and CA1 region. These sections are shown at higher magnification in Supplementary Figs 1 and 2. Scale bars: **A–D** = 1600 μm. GD = dentate gyrus.

spines of basal dendrites from PHF-tau$^-$ neurons and PHF-tau$^+$ neurons, in the parahippocampal cortex of Patient P9 and CA1 of Patients P9, P13 and P14.

Lucifer yellow-injected neurons with Pattern I of immunostaining for paired helical filament-tau

Of the 96 neurons injected in layer III of the parahippocampal cortex of Patient P9, 83 were PHF-tau$^-$ neurons, and 13 were PHF-tau$^+$ neurons. We analysed 12 dendrites from different PHF-tau$^-$ and 12 dendrites from PHF-tau$^+$ neurons (Supplementary Table 1). We did not find any significant differences between PHF-tau$^-$ and PHF-tau$^+$ neurons in terms of dendrite diameter, dendritic spine density, or the length and volume of the dendritic spines in function of the distance from the soma (Supplementary Fig. 6 and see Supplementary Table 2 for the average values of these parameters). Furthermore, no differences were found in the frequency distribution of spine length (2577 and 2391 dendritic spines, respectively) and spine volume (2584 and 2394 dendritic spines, respectively) between PHF-tau$^-$ and PHF-tau$^+$ neurons (Supplementary Fig. 6I and J).

Lucifer yellow-injected neurons with Pattern IIa of immunostaining for paired helical filament-tau

Of the 40, 62 and 48 neurons in the CA1 of Patients P9, P13 and P4 injected with Lucifer yellow, 34, 48 and 33 were PHF-tau$^-$

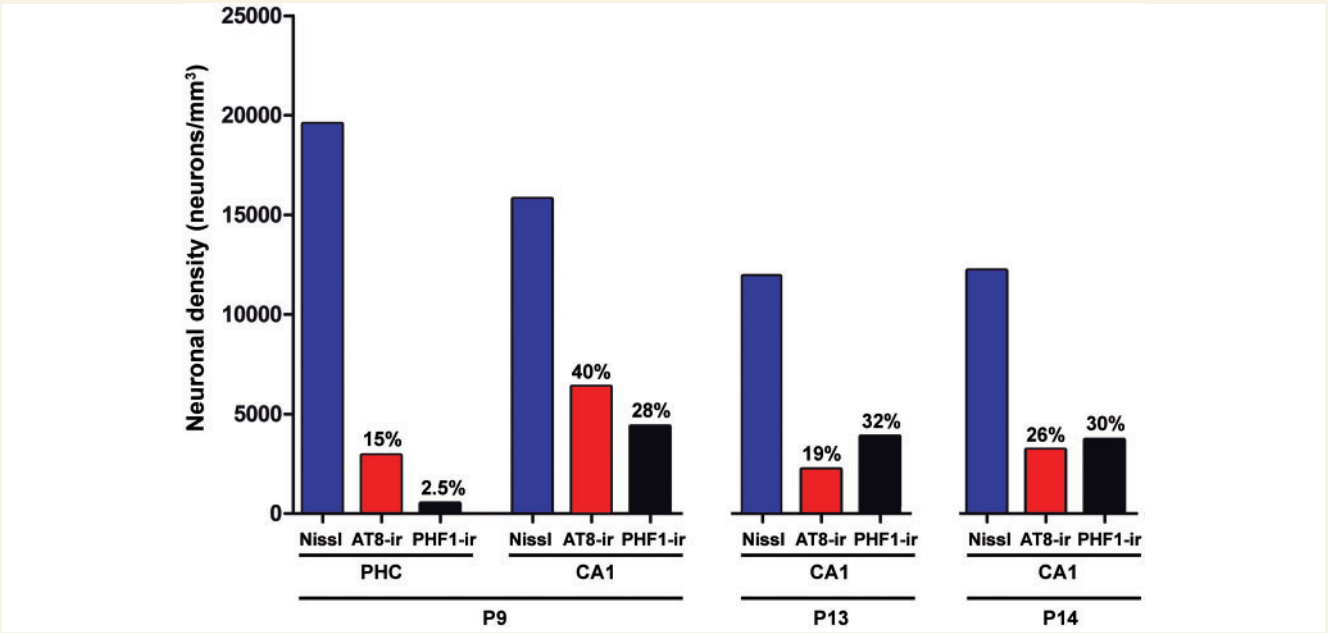

Figure 2 Neuronal density. Graph showing the neuronal density in the parahippocampal cortex and CA1 regions of Patients P9, P13 and P14. Blue columns: total neuron density; red columns: PHF-tau$_{AT8}$-ir neuron density; black columns: PHF-tau$_{PHF-1}$-ir neuron density. The percentages indicated at the top of the red and black columns represent the percentage of phospho-tau neurons with respect to the total neuron density in each region.

neurons, respectively, while the remainder were labelled for PHF-tau$_{AT8}$-ir or PHF-tau$_{PHF-1}$-ir. We analysed six, five and five dendrites from different PHF-tau$^-$ neurons and nine, eight and six dendrites from different PHF-tau$^+$ neurons in Patients P9, P13 and P14, respectively (Supplementary Table 1).

Dendrite diameter

There were no significant differences in dendrite diameter as a function of the distance from the soma between the PHF-tau$^-$ and PHF-tau$^+$ neurons from Patients P9, P13 and P14 (Supplementary Fig. 7A, C and E). In Patient P9, the average dendrite diameter did differ significantly between the two groups of neurons, the dendrites of PHF-tau$^+$ neurons having a 22% smaller diameter than in PHF-tau$^-$ neurons (Supplementary Fig. 7B and Supplementary Table 2). However, no such differences were found in the neurons from Patients P13 and P14 (Supplementary Fig. 7D and F; Supplementary Table 2).

Dendritic spine density

The analysis of the dendritic spine density as a function of the distance from the soma revealed no statistical differences between PHF-tau$^-$ and PHF-tau$^+$ neurons in Patient P9 (Fig. 7A and B). By contrast, in Patients P13 and P14 we found statistical differences between PHF-tau$^-$ and PHF-tau$^+$ neurons in the medial/distal portions (Fig. 7C and E), and similar results were found when the data are presented as the average (Fig. 7D and F; Supplementary Table 2).

Dendritic spine length

In Patients P9, P13 and P14, the length of the dendritic spines in function of their distance from the soma was similar between PHF-tau$^-$ (2234, 2267 and 3213 dendritic spines, respectively) and PHF-tau$^+$ neurons (2225, 2281 and 2310 dendritic spines, respectively: Fig. 8A, D and G; Supplementary Table 2). The average dendritic spine length decreased significantly in Patient P9 (14%, Fig. 8B), whereas no differences were found in Patients P13 and P14 (Fig. 8E and H; Supplementary Table 2). The frequency distribution revealed a higher frequency of shorter dendritic spines in PHF-tau$^+$ neurons from Patients P9 and P13 (Fig. 8C and F), whereas in Patient P14 short dendritic spines were less frequent on PHF-tau$^+$ neurons than PHF-tau$^-$ neurons (Fig. 8I).

Dendritic spine volume

In Patients P9, P13 and P14, the volume of the dendritic spines as a function of their distance from the soma did not differ between PHF-tau$^-$ (2266, 2262 and 3217 dendritic spines, respectively) and PHF-tau$^+$ neurons (2250, 2276 and 2300 dendritic spines, respectively; Fig. 8J, K, M, N, P and Q; Supplementary Table 2). However, there were significant differences in the frequency distribution of the volume of dendritic spines for all cases, whereby small dendritic spines were more frequent in PHF-tau$^+$ neurons than in PHF-tau$^-$ neurons (Fig. 8L, O and R).

In summary, all the morphological parameters of dendrites from Lucifer yellow-injected PHF-tau$^+$ (Pattern I) pyramidal neurons in layer III of the parahippocampal cortex remained unchanged when they were compared with the dendrites of Lucifer yellow-injected pyramidal neurons that were PHF-tau$^-$ in the same cortical area. In the CA1, all the PHF-tau$^+$ Lucifer yellow-injected pyramidal neurons that were analysed quantitatively showed Pattern IIa immunostaining. The presence of tau aggregates forming intraneuronal neurofibrillary tangles in these neurons gives rise to changes in

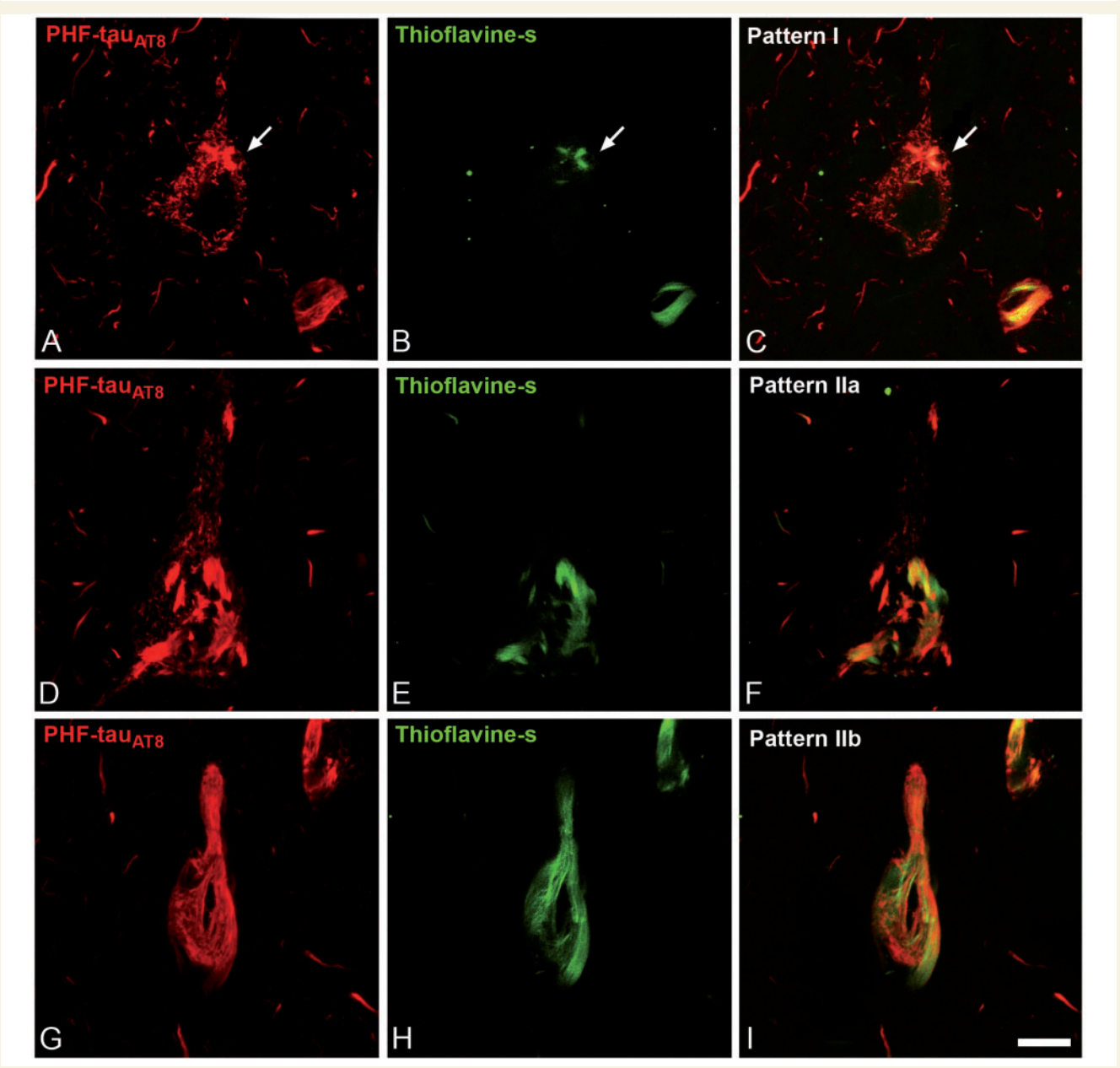

Figure 3 Patterns of PHF-tau immunostaining. Confocal microscopy images showing neurons in parahippocampal cortex (**A–C**) and CA1 (**D–I**) double-stained with PHF-tau$_{AT8}$ (red) and thioflavin S (green) (**D–I**) to illustrate Pattern I (neuron indicated with an arrow), Pattern IIa and Pattern IIb of immunostaining. Scale bars: **A–I** = 10 μm.

the morphology of dendritic spines (smaller volume and shorter length) in all patients, although dendritic spines were only lost in Patients P13 and P14. However, the density of neurons in the CA3 was lower in these latter patients than in Patient P9 (38% and 42% fewer neurons, respectively), suggesting that the CA3 pathology was more advanced in these patients than in Patient P9 (Supplementary material). Because CA3 is a major source of synaptic inputs to the CA1 (the Schaffer collateral projection), it is possible that the loss of these synaptic inputs may contribute to a loss of dendritic spines in the CA1 of these patients. Finally, neurons that had developed extreme neurofibrillary tangles (Pattern IIb) displayed a reduced dendritic arbor and few or virtually no dendritic spines (Fig. 6). The dendritic diameter was also remarkably thin in all of these cases.

Other morphological alterations

In addition to the soma and proximal processes, PHF-tau$_{AT8}$ was also found in the distal dendritic segments of Lucifer yellow-injected neurons. Interestingly, except for one dendrite, the distal dendritic segments of PHF-tau$_{AT8}$–ir neurons that showed Pattern I were not stained by the antibody. However, we observed the presence of fibrillar PHF-tau$_{AT8}$ staining in the majority of the distal portions of dendrites from PHF-tau$_{AT8}$–ir neurons with

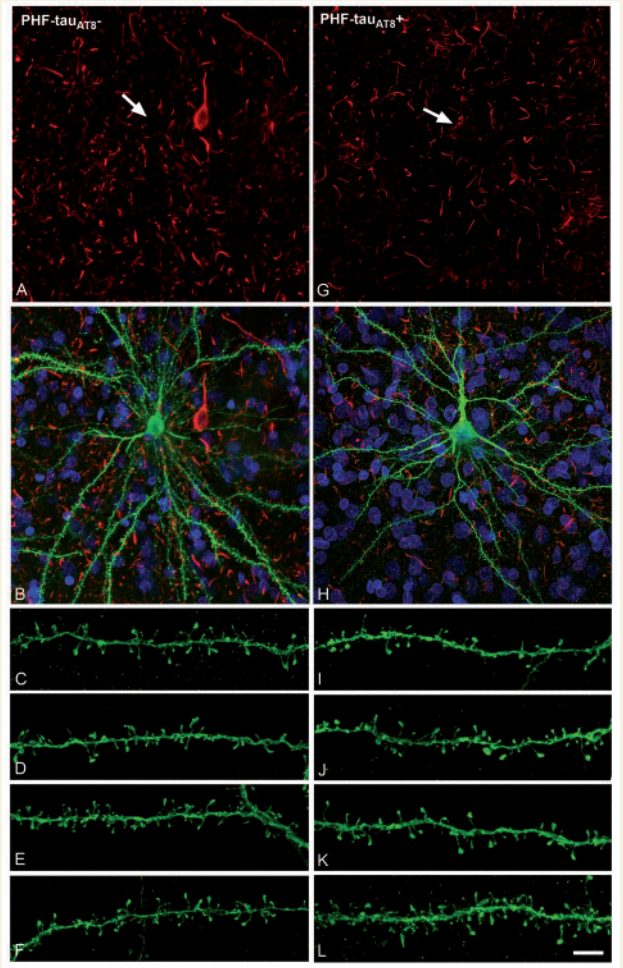

Figure 4 PHF-tau$^-$ neurons and neurons with Pattern I PHF-tau$_{AT8}$ staining. Neurons and dendrites in the parahippocampal cortex of Patient P9 injected with Lucifer yellow whose soma is free of PHF-tau$_{AT8}$-ir (PHF-tau$^-_{AT8}$; **A–F**) or that contains PHF-tau$_{AT8}$ in the putative pre-tangle state (Pattern I; **G–L**). Stacks of 26 (**A** and **B**) and 28 (**G** and **H**) images, respectively, obtained after combining the channels acquired separately for DAPI (blue), Lucifer yellow (green) and PHF-tau$_{AT8}$ immunostaining (red). (**C–L**) Stacks of 26–32 confocal optical sections from basal dendrites of PHF-tau$^-_{AT8}$ (**C–F**) and immunostained (PHF-tau$^+_{AT8}$; **I–L**) Lucifer yellow-injected pyramidal neurons. The cell bodies of the neurons in **B** and **H** are shown at higher magnification in Supplementary Fig. 3A–F and G–L, respectively. These PHF-tau$^-_{AT8}$ and PHF-tau$^+_{AT8}$ Lucifer yellow-injected neurons were recovered and reprocessed immunocytochemically using anti-PHF-tau$_{PHF\text{-}1}$. The PHF-tau$^-_{AT8}$ neuron was non-immunostained for PHF-tau$_{PHF\text{-}1}$ (PHF-tau$^-$). Scale bars: **A**, **B**, **G** and **H** = 13 μm; **C–F** and **I–L** = 2 μm.

Pattern IIa staining (Supplementary Fig. 8). In these distal dendritic regions with fibrillar PHF-tau$_{AT8}$, the dendritic spine density was analysed in Patient P9. When these segments were compared with adjacent segments of the same length (pre-terminal segments lacking PHF-tau$_{AT8}$) there was a significantly lower density of dendritic spines in the distal dendritic regions with fibrillar PHF-tau$_{AT8}$ (Supplementary Fig. 9) than in the pre-terminal segments. This result is suggestive of a local toxic effect, since the density of dendritic spines in the pre-terminal dendritic segment was similar to that found in dendrites lacking PHF-tau$_{AT8}$.

Discussion

In the present study, we found no significant changes in the microanatomy of dendrites from pyramidal neurons at early stages of a neurofibrillar pathology, as defined by the presence of diffuse phospho-tau in a putative pre-tangle state (Pattern I). However, once tau aggregates of neurofibrillary tangles had formed (Patterns IIa and IIb), representing more advanced neurofibrillar alterations, significant reductions in the diameter of dendrites and in the number, length and volume of spines were evident. The severity of these changes seems to be progressive, from the intermediate/advanced stages (Pattern IIa) to extreme stage (Pattern IIb) of the neurofibrillar pathology.

Methodological considerations

The main aim of the study was to compare the microanatomy of cortical pyramidal cells between those free of signs of any neurofibrillar pathology (PHF-tau$^-$ neurons) and those showing either diffuse phospho-tau (putative pretangle state) or aggregated tau neurofibrillary tangles in different cortical regions.

However, there are important drawbacks in carrying out such a study that must be taken into consideration. First, the total number of cells that can be injected is relatively low since it takes ~10 min to inject a cell and the best injections are obtained within a time window of 24–48 h after fixation. Second, pyramidal cells in different cortical regions have considerably distinct structures (Elston *et al*., 2001; Jacobs *et al*., 2001) and the data obtained in one region cannot necessarily be applied to another. Thus, the microanatomy of pyramidal cells must be examined separately in different regions. Third, the morphological alterations observed in human pathological tissue are very difficult to interpret due to the high interindividual variability (sex, age, medical treatment, etc.), factors that could affect brain structure. Accordingly, one must be careful to avoid interpreting normal interindividual characteristics as morphological alterations, or changes as a consequence of a medical treatment or any other factor. In addition, the course such diseases take is highly variable as the neuropathological changes are not homogenous, neither among patients nor in different regions of the brain of the same patient, giving rise to variation in the alterations to cortical circuits (Garcia-Marin *et al*., 2009; Blazquez-Llorca *et al*., 2010). Furthermore, dendrites in contact with amyloid-β plaques suffer changes in the number and morphology of their spines (Tsai *et al*., 2004; Spires *et al*., 2005; Knafo *et al*., 2009*a*, *b*; Merino-Serrais *et al*., 2011). Thus, it is critical to use neurons not affected by the neurofibrillar and amyloid-β pathology (i.e. neurons whose dendrites are not in contact with amyloid-β plaques) from the same individual when studying how abnormal phosphorylation of tau influences the microanatomy of pyramidal neurons. Indeed, these PHF-tau$^-$ neurons were located adjacent

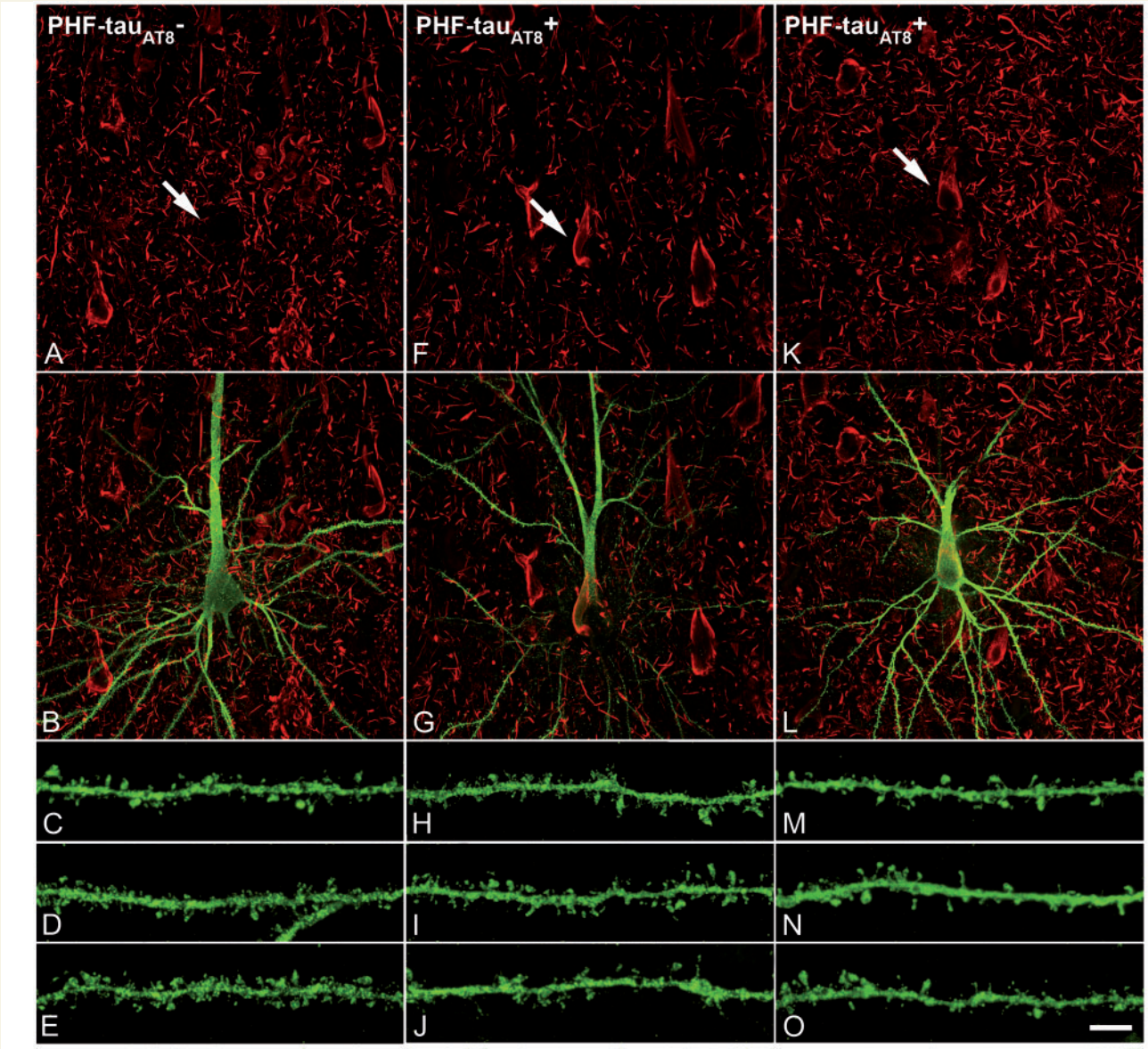

Figure 5 PHF-tau^{-} and neurons with Pattern IIa PHF-tau$_{AT8}$ staining. Neurons and dendrites in the CA1 of Patients P14 (**A–J**) and P13 (**K–O**), injected with Lucifer yellow, and with a soma free of PHF-tau$_{AT8}$ (PHF-tau$_{AT8}^{-}$; **A–E**) or with PHF-tau$_{AT8}$–ir tangles (Pattern IIa; **F–O**). (**A–B**, **F–G** and **K–L**) Stacks of 18 and 35 images, respectively, obtained after combining the channels acquired separately for Lucifer yellow (green) and PHF-tau$_{AT8}$ (red). (**C–D**, **H–J** and **M–O**) Stacks of 26–58 optical confocal sections of the basal dendrites of PHF-tau$_{AT8}^{-}$ (**A** and **B**) and immunostained (PHF-tau$_{AT8}^{+}$; **F–G**, **K–L**) Lucifer yellow-injected pyramidal neurons. These PHF-tau$_{AT8}^{-}$ and PHF-tau$_{AT8}^{+}$ Lucifer yellow-injected neurons were recovered and reprocessed immunocytochemically using anti-PHF-tau$_{PHF\text{-}1}$. The PHF-tau$_{AT8}^{-}$ neuron was non-immunostained for PHF-tau$_{PHF\text{-}1}$ (PHF-tau^{-}), whereas the PHF-tau$_{AT8}^{+}$ neurons were also PHF-tau$_{PHF\text{-}1}$ (Supplementary Fig. 5). Scale bars: **A**, **F** and **K** = 10 μm; **C–E**, **H–J** and **M–O** = 3 μm.

to those showing phospho-tau and with dendrites located in plaque-free regions. In addition, it is not possible to know which neurons have developed a neurofibrillar pathology before injection and hence, the proportion of cells showing a neurofibrillar pathology is rather unpredictable. As a consequence, the ideal conditions to perform a detailed quantitative study would be to obtain sufficient cells with and without neurofibrillar pathology in different regions of the same patient. These conditions were met in Patients P9, P13 and P14.

Finally, it should be noted that there are several methods to visualize dendritic spines in the human brain. A common method is the Golgi technique but this is inconsistent and incomplete. Another method involving intracellular injections of marker substances in fixed brain tissue is currently considered the best approach to visualize the dendritic spines in the human brain and is a well-established technique (Einstein, 1988; Buhl *et al*., 1990). The fact that neurons with well-developed tangles do not have dendritic spines or have very few compared with other neurons with

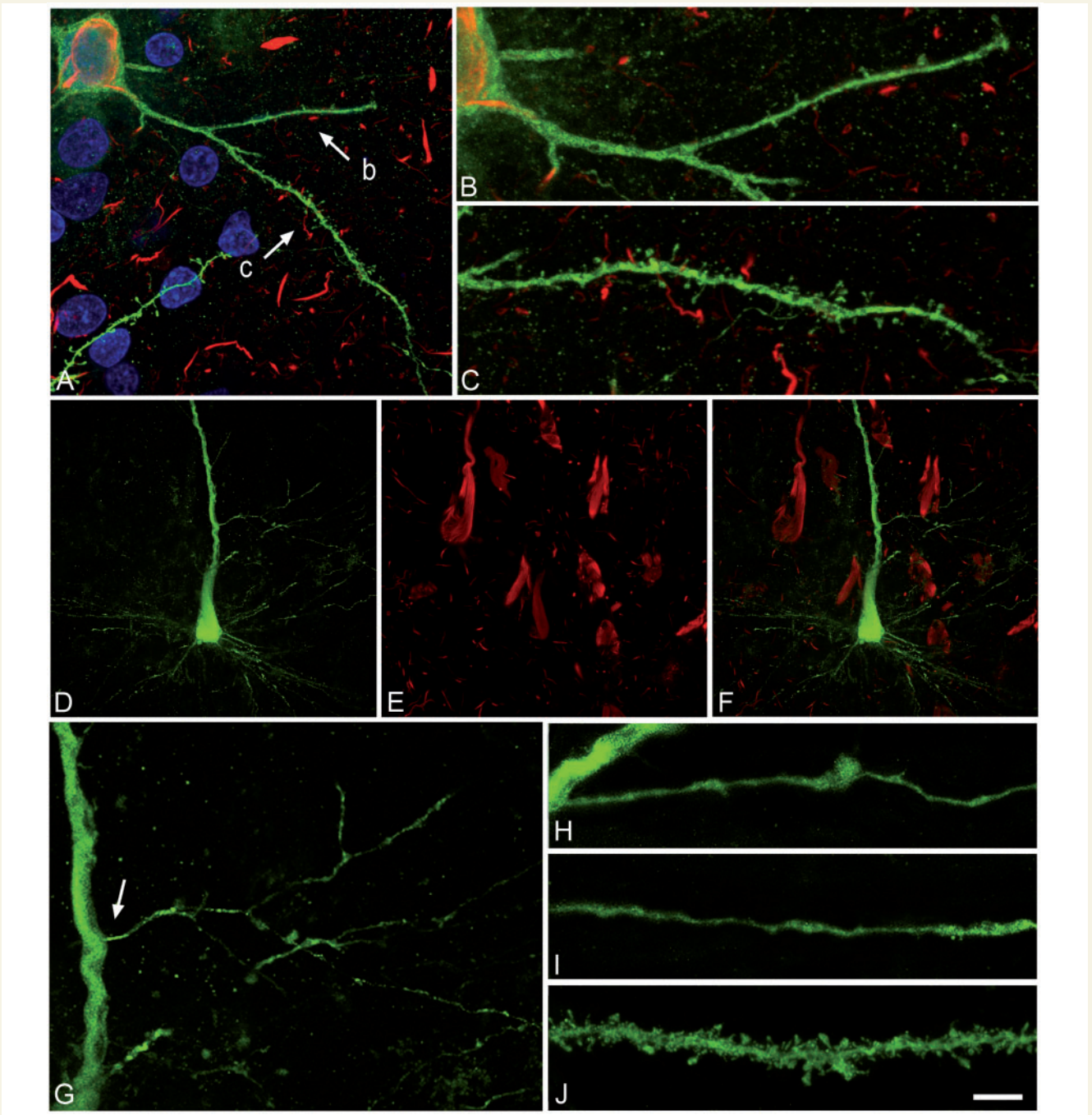

Figure 6 Neurons with Pattern IIb of PHF-tau immunostaining. Alterations of dendrites and dendritic spines in Lucifer yellow injected neurons with Pattern IIb PHF-tau$_{AT8}$-ir from layer III of the parahippocampal cortex in Patient P9 (**A–C**) and Pattern IIb PHF-tau$_{PHF\text{-}1}$-ir in the CA1 of Patient P12 (**D–L**). (**A**) Stack of 27 confocal optical sections obtained after combining the channels acquired separately for DAPI (blue), Lucifer yellow (green) and PHF-tau$_{AT8}$-ir (red), showing the cell body and proximal dendrites of the intracellular labelled neuron with Pattern IIb PHF-tau$_{AT8}$–ir. (**B** and **C**) Higher magnification of **A**, showing the dendrites indicated as 'b' and 'c', respectively. Note the low density of dendritic spines in dendrite 'b' compared with dendrite 'c', and in the latter dendrite compared with the dendrites in Figs 4 and 5. Also, the dendritic spines are notably smaller. (**D–E**) Stacks of 27 confocal optical sections showing the cell body and proximal dendrites of the intracellular labelled neuron (**D**) with Pattern IIb PHF-tau$_{PHF\text{-}1}$–ir (**E**). (**F**) Image obtained by combining **D** and **E**. (**G**) Higher magnification of **D**. (**H** and **I**) Stacks of 38–55 confocal optical sections from a collateral apical dendrite (arrow in **G**) of the Lucifer yellow-injected pyramidal neuron, showing different segments of the same dendrite (**H**, proximal; **I**, distant). (**J**) Stack of 26 confocal optical sections from the collateral apical dendrite of an intracellular labelled neuron that was adjacent to the Lucifer yellow-injected neuron shown in **D**, and that was not PHF-tau$_{PHF\text{-}1}$–ir. Note the lack of dendritic spines and the thin diameter of the dendrites of the PHF-tau$_{PHF\text{-}1}$-ir neuron (**H** and **I**) compared with the dendrite of the PHF-tau^{-} neuron (**J**). Scale bars: **A** = 10 μm**; B** and **C** = 3.5 μm; **D–F** = 20 μm; **G** = 9 μm; **H–J** = 4.5 μm.

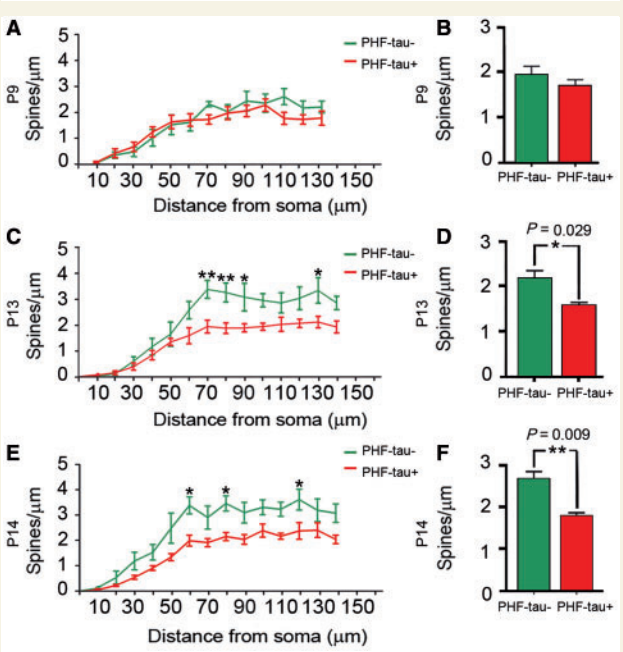

Figure 7 Dendritic spine density. Comparative morphometric analysis of dendrites from Lucifer yellow-injected PHF-tau$^+$ pyramidal neurons and dendrites from Lucifer yellow-injected PHF-tau$^-$ neurons in the CA1 of Patient P9 (**A** and **B**), Patient P13 (**C** and **D**) and Patient P14 (**E** and **F**). (**A**, **C** and **E**) Dendritic spine density (dendritic spines/µm) in function of the distance from soma. (**B**, **D** and **F**) Average dendritic spine density per dendrite. $*P < 0.05$; $**P < 0.01$.

less developed tangles in the same regions and in the same patients is therefore interpreted as a decrease or loss of dendritic spines. This interpretation is also supported by a large number of researchers who study dendritic spine alterations both in humans and animal models (see Penzes *et al.*, 2011; Spires-Jones and Knafo, 2012 for recent reviews).

Patterns of paired helical filament-tau immunostaining and alterations to pyramidal cell dendrites

At the cellular level, abnormal tau phosphorylation and the formation of tangles are major events in neuronal degeneration in Alzheimer's disease (Grundke-Iqbal *et al.*, 1986). It is well known that some neurons are not affected in any of the cortical regions damaged in Alzheimer's disease, whereas others are altered to a different degree. Such variation could reflect different steps in the process of neuronal degeneration. A marker for this degeneration is tau phosphorylation at the site recognized by the antibody AT8 (PHF-tau$_{AT8}$). This may be a suitable marker for the initial steps of degeneration, as increased tau aggregation can subsequently be found in some neurons and it can be readily visualized with the PHF-1 tau antibody (PHF-tau$_{PHF\text{-}1}$). However, how this degeneration is triggered and progresses remains unknown (Avila *et al.*, 2012).

It has been proposed that in the early disease stages, neuronal loss commences in the hippocampal formation and that it may reflect the impairment of adult neurogenesis in the dentate gyrus (Li *et al.*, 2008). Newborn neurons form functional synapses with CA3 neurons, and the axons emitted by dentate gyrus neurons generated in the adult form synapses with the thorny excrescences of CA3 neurons (Toni *et al.*, 2008). We recently showed that there is a selective yet conspicuous abnormal phosphorylation of tau in the thorny excrescences of hippocampal CA3 neurons in a putative pre-tangle state from patients with Alzheimer's disease (Pattern I PHF-tau$_{AT8}$-ir). Thus, we suggested this alteration might be a very early marker of disease onset, possibly representing the first step in impaired synaptic transmission (Blazquez-Llorca *et al.*, 2011). Since thorny excrescences are key structures in the synaptic pathway that transfers neocortical representations to the hippocampus (Andersen *et al.*, 2007), it is possible that these structures may play an essential role in the early memory impairment typical of patients with Alzheimer's disease.

As reported previously (Bancher *et al.*, 1989; Braak *et al.*, 1994; Blazquez-Llorca *et al.*, 2010), we have used the PHF-tau$_{AT8}$ antibody to classify neurons with different phosphorylated and aggregated patterns of tau (fibrillar aggregates and typical neurofibrillary tangles). Initially, no phosphorylation and no aggregation are observed but subsequently, neurons stained for PHF-tau$_{AT8}$ can be divided into neurons showing Pattern I (diffuse cytoplasmic staining) or Pattern II (in which typical neurofibrillary tangles are evident).

Neurons with Patten I displayed some positivity with thioflavin S (Fig. 3). In general, it is considered that staining with thioflavin S would preclude the use of the term 'pre-tangle' to classify a neuron that is positive for thioflavin S. Indeed, it has been shown that this dye binds to PHF with a higher affinity than to the straight filaments but the staining with thioflavin S indicates a higher content of β-sheet in the secondary structure of tau protein. This change to a β-sheet conformation could occur in oligomers and they do not require the presence of tau filaments (Santa-María *et al.*, 2006). Furthermore, the maturation of the neuronal fibrillar tau inclusions is a continuous process that can be examined using thioflavin S stain or other dyes (Mohorko *et al.*, 2010). In the first stage, which is often referred to as the pre-tangle stage, accumulation of phospho-tau is thought to begin in the cytoplasm and is still predominantly non-fibrillar. Thus, in this stage, the observation of some small fibrillar tau inclusions would be expected with thioflavin S. It is important to point out that the identification of these neurons is difficult with thioflavin S alone, as the small size of the fibrillar aggregates does not outline the silhouette of the cell body. The intermediate stage is characterized by mature neurofibrillary tangles, in which phospho-tau is aggregated in large intracellular tightly packed fibrils, making it more feasible to identify the overall structure as a neuron with neurofibrillary tangle. The final stage is characterized by the so-called ghost tangles that are present outside cells when the cells have died. For these reasons we considered Pattern I as a putative pre-tangle stage in spite of the fact that these neurons may show some small intracellular thioflavin S positive inclusions.

In the present study, Pattern II was subdivided into Patterns IIa and IIb, depending on the development of neurofibrillary tangles

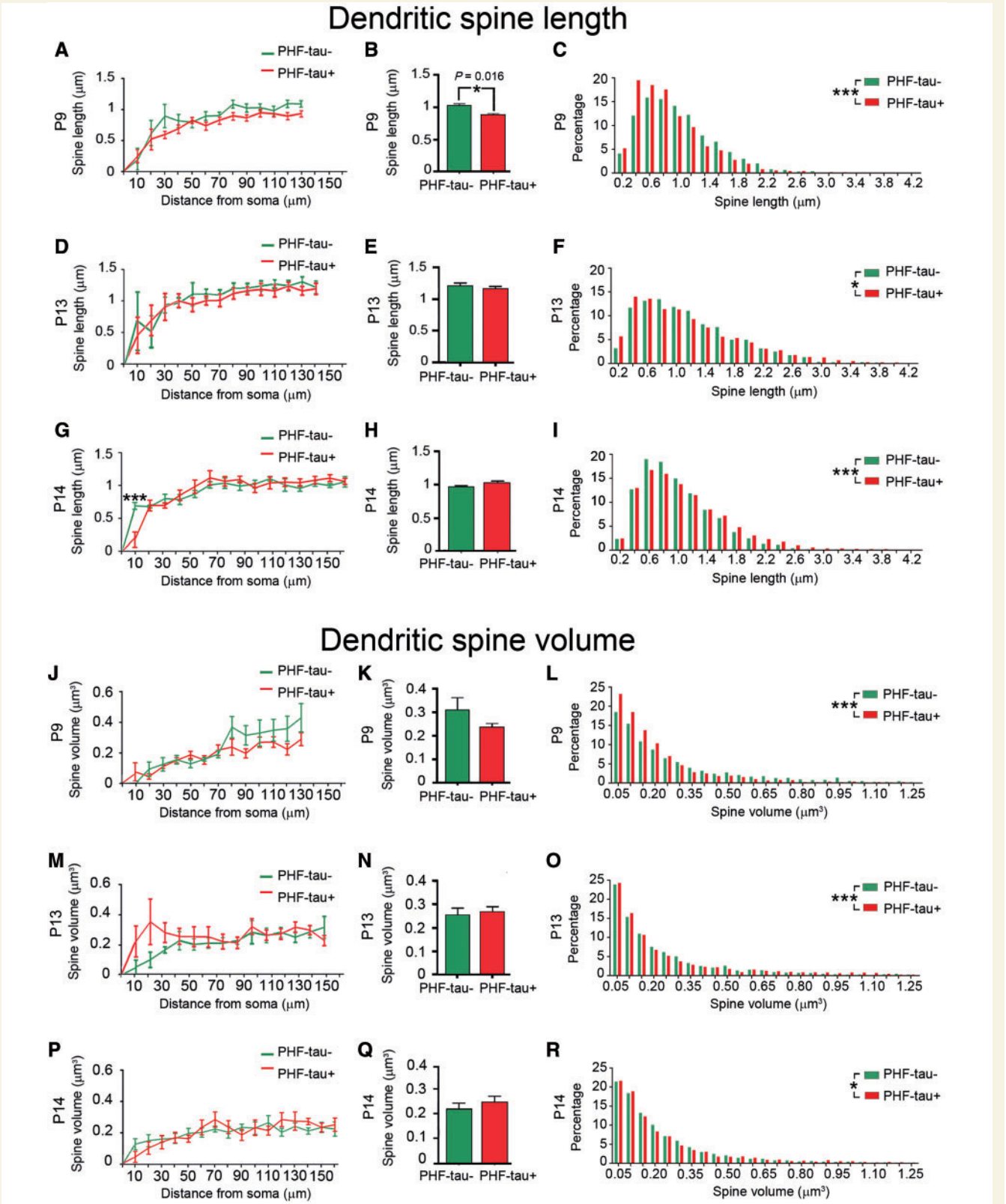

Figure 8 Morphometric analysis. Comparative morphometric analysis of dendritic spine length (**A–I**) and dendritic spine volume (**J–R**) for Lucifer yellow-injected PHF-tau$^+$ pyramidal neurons and Lucifer yellow-injected PHF-tau$^-$ neurons from the CA1 of each patient in function of the distance from soma (**A**, **D**, **G**, **J**, **M** and **P**). The average per dendrite (**B**, **E**, **H**, **K**, **N** and **Q**) and the frequency distribution (**C**, **F**, **I**, **L**, **O** and **R**) are shown: $*P < 0.05$; $**P < 0.01$; $***P < 0.001$.

(Pattern IIa, intermediate/advanced; Pattern IIb, extreme). However, the most prominent staining of neurons with neurofibrillary tangles was observed with the PHF-1 antibody. Indeed, the vast majority of PHF-tau$_{PHF-1}$-ir neurons had a large amount of aggregated tau, consistent with the hypothesis that PHF-tau$_{AT8}$ mostly labels the initial stages of a neurofibrillar pathology, while PHF-tau$_{PHF-1}$ recognizes the later stages (Blazquez-Llorca *et al.*, 2011).

Neurons showing each of these phospho-tau patterns were analysed for possible alterations to their dendritic spines. As summarized in Fig. 9, no changes were found in the number, length or volume of the dendritic spines in neurons with Pattern I, nor in dendrite diameter, whereas several significant alterations were found in neurons showing Pattern II. At the intermediate level of a neurofibrillar pathology (Pattern IIa), we found different morphological alterations depending on the patients, mostly a reduction in dendritic spine volume and length (Patient P9) and a reduction in dendritic spine density (Patients P13 and P14). At late stages (Pattern IIb), there was a dramatic loss of spines, even in the proximal portion of the dendrites. This sequential loss of dendritic spines appears to be distinct to that found in the presence of amyloid-β plaques, where the dendritic regions close to the extracellular plaques are depleted of dendritic spines irrespective of whether they are proximal or distal to the soma (Knafo *et al.*, 2009*a*). However, there seems to be a sequence related to the loss of dendritic spines in association with the intracellular tau pathology, occurring first in the distal and then in the more proximal regions (Fig. 9).

It is not clear whether Pattern I represents a pre-tangle stage and therefore precedes Pattern II, or if this just occurs in a subpopulation of these neurons representing an independent stage. Because all Lucifer yellow-injected neurons with neurofibrillar pathology examined here were immunostained for PHF-tau$_{AT8}$ or PHF-tau$_{PHF-1}$, we do not know whether the changes found in the microanatomy of these neurons are characteristic of a particular subpopulation of neurons or similar changes occur in neurons with other phosphorylated tau epitopes. Certainly, neurons with well-developed neurofibrillary tangles (Pattern IIb) had a relatively small dendritic tree, with thin dendrites and very few or no spines,

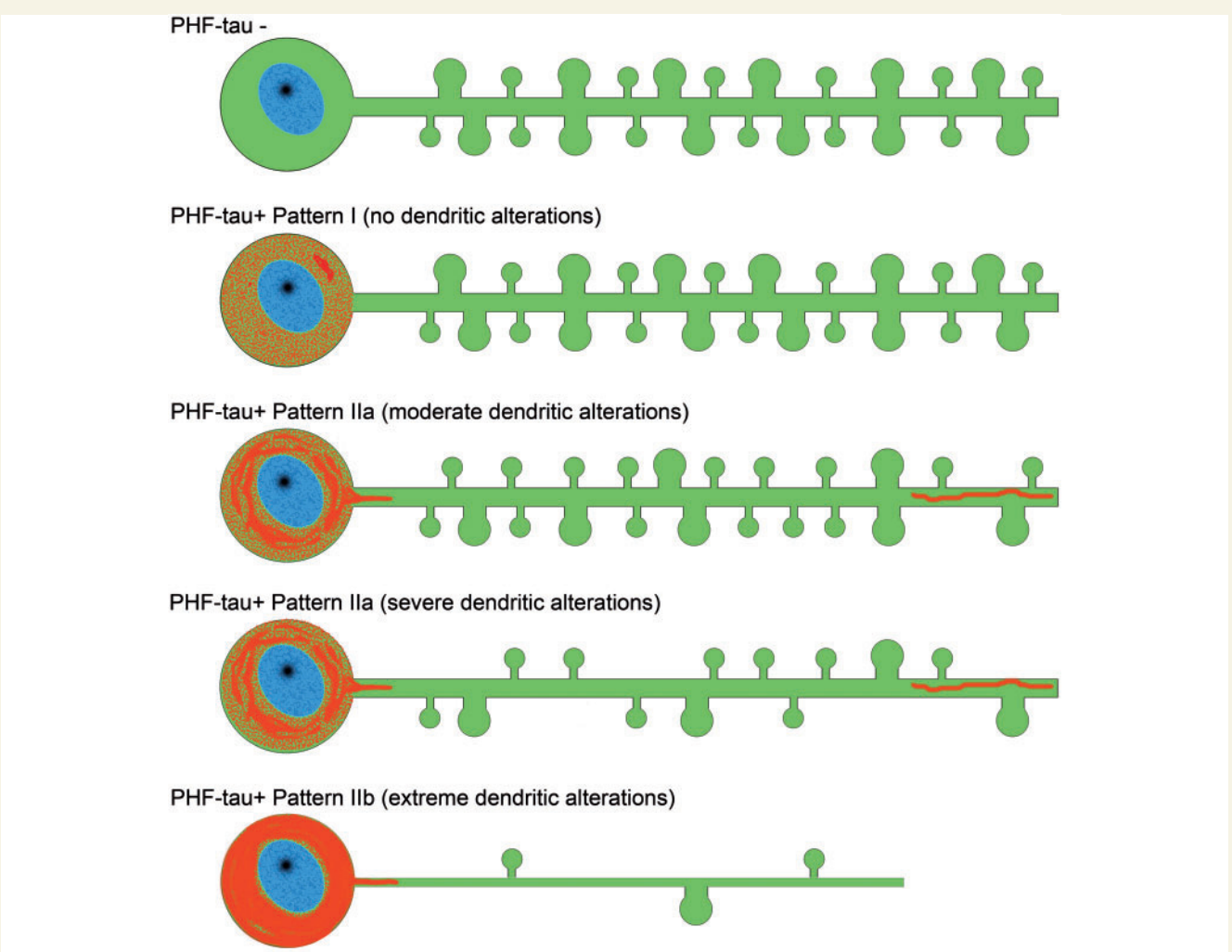

Figure 9 Scheme representing the changes to dendrites of Lucifer yellow-injected neurons that showed different patterns of PHF-tau immunostaining. For simplicity, dendritic spines were represented as two types: small and large. Red = phospho-tau.

regardless of whether they were PHF-tau$_{AT8}$-ir or PHF-tau$_{PHF-1}$-ir. Further experiments would be necessary to analyse the microanatomy of neurons with other phosphorylated tau epitopes.

Possible functional implications of the morphological changes observed

Dendrite diameter

There was a decrease in the dendrite diameter in PHF-tau$^+$ neurons showing Patterns IIa and IIb, although we do not know if this reduction selectively affects some organelles or if it only represents a decrease in cytosolic volume. In any case, the change in dendrite diameter is likely to affect the physiological activity of the neuron as dendrite diameter is closely related to electrical conductivity (Holmes, 1989; Mainen and Sejnowski, 1996; Vetter *et al*., 2001). Thus, changes in diameter may produce functional alterations.

Morphology of dendritic spines

In animal models, changes in the neck length of dendritic spines affects the temporal compartmentalization of calcium and other second messengers, changes that may affect the induction of long-term potentiation (Yuste, 2010; Bloodgood and Sabatini, 2005). Additionally, the volume of the dendritic spine head is related to the size of the postsynaptic density (Harris and Stevens, 1989; Schikorski and Stevens, 1997; Arellano *et al*., 2007*b*), the number of presynaptic vesicles, and the number of vesicles adjacent to the presynaptic cleft (Harris and Stevens, 1989). The area of the postsynaptic density is proportional to the number of postsynaptic receptors (Nusser *et al*., 1998), while the number of vesicles adjacent to the presynaptic cleft is proportional to those primed for synaptic transmitter release (Dobrunz and Stevens, 1997). Furthermore, the volume of the head is directly proportional to the strength of synaptic currents (Harris and Stevens, 1989; Schikorski and Stevens, 1997; Arellano *et al*., 2007*a*). Therefore, the morphology of a dendritic spine determines its synaptic strength and learning rules. Hence, the changes observed in the volume and length of dendritic spines in the present study are likely to have important functional consequences.

Density of dendritic spines

Assuming the hypothesis that one spine corresponds to one excitatory synapses (Arellano *et al*., 2007*b*), differences in the number of dendritic spines probably reflect differences in the number of excitatory inputs that a cell can integrate. Dendritic spines on pyramidal cells are the recipients of most excitatory inputs to the cerebral cortex (DeFelipe and Fariñas, 1992) and thus, the loss of dendritic spines indicates a synaptic disconnection that must certainly have an important consequence in the cognitive attributes of the patients with Alzheimer's disease.

Nevertheless, we observed that in neurons showing an intermediate state of neurofibrillar pathology (Pattern IIa) there is not necessarily a loss of dendritic spines, since substantial reductions in the density of dendritic spines on CA1 pyramidal neurons with Pattern IIa was observed in Patients P13 and P14 but not in Patient P9. Importantly, the density of CA3 neurons in Patient P9 was 14 350 neurons/mm^3, whereas there were only 8916 neurons/mm^3 and 8447 neurons/mm^3 in Patients P13 and P14, respectively (Supplementary material), suggesting that the CA3 region in the latter two patients is more pathologically affected than that of Patient P9. Since CA3 pyramidal cells project strongly to the dendritic spines of CA1 pyramidal neurons (the Schaffer collateral projection; Andersen *et al*., 2007), it is possible that the decrease in dendritic spine density on CA1 neurons in Patients P13 and P14 could be due to a loss of excitatory inputs from Schaffer collaterals rather to the presence of neurofibrillary tangles. Thus, it is important to consider the role of phospho-tau.

Paired helical filament-tau: neuroprotection or toxicity

Tau protein has ~80 known phosphorylatable sites (Hanger *et al*., 2009) and it is a matter of debate whether modification of the protein at specific sites could have protective or toxic consequences for the neuron where modified tau is present (Alonso *et al*., 2001, 2010; Lee *et al*., 2005; Wang *et al*., 2007; Castellani *et al*., 2008; Wang and Liu, 2008). On the one hand it is thought that the soluble forms of PHF-tau (diffuse staining) have a toxic effect, since they abduct normal tau and other microtubule-associated proteins, thereby producing the disassembly of microtubules that are responsible for axonal transport and possibly causing a loss of synapses (Iqbal *et al*., 2005). However, it was also proposed that the soluble PHF-tau protein associates to form neurofibrillary tangles, removing cytosolic soluble PHF-tau and serving as a neuroprotective mechanism (Andorfer *et al*., 2003; Santacruz *et al*., 2005; Alonso *et al*., 2006; Spires-Jones *et al*., 2008; Iqbal *et al*., 2009). However, neurofibrillary tangles appear to be toxic since they are associated with impaired axonal transport, which provokes cell death (Stamer *et al*., 2002; Terwel *et al*., 2002; Cente *et al*., 2006; Smith *et al*., 2007). Indeed, there are studies suggesting a strong correlation between the loss of synaptic markers and the presence of neurofibrillary tangles (Terry *et al*., 1991; Honer *et al*., 1992; Masliah *et al*., 1992; Wakabayashi *et al*., 1994; Lue *et al*., 1996; Samuel *et al*., 1997; Heffernan *et al*., 1998). Our results indicate that neurons with advanced neurofibrillary tangles display a remarkable loss of dendritic spines, which is consistent with other studies. However, it should be emphasized that the presence of PHF-tau$_{AT8}$ or PHF-tau$_{PHF-1}$ is not necessarily associated with a loss of dendritic spines, even in intermediate stages of a neurofibrillar pathology. These observations suggest that neurons in a putative pre-tangle stage or with neurofibrillary tangles in intermediate stages may not be affected (or they may be only slightly affected) or they may be in a reversible state.

Studies on the European ground squirrel demonstrated that PHF-like phosphorylation is induced in the brain during the hibernation of these animals (Arendt *et al*., 2003), which is similar to the characteristic increase in tau phosphorylation (Avila *et al*., 2004). Furthermore, changes in the denervation/reinnervation of CA3 pyramidal neurons by mossy fibres were also found during hibernation/arousal (Popov and Bocharova, 1992) and they were associated with a reversible PHF-like phosphorylation of tau over a similar time course. Thus, it was proposed that the formation and degradation of PHF-like tau might represent a physiological mechanism not necessarily associated with pathological effects but

rather, with neuronal plasticity. Here, a reduction in the density of dendritic spines in the distal segments commonly accompanied the accumulation of fibrillar phospho-tau$_{AT8}$. Assuming that the majority of the dendritic spines establish synapses (Arellano *et al*., 2007*b*), our results suggest that the distal segments of these neurons are disconnected, unlike the rest of the dendritic tree. However, we cannot discard physiological or molecular alterations in synaptic transmission due to the morphological changes observed in the dendritic spines.

Finally, Lucifer yellow-injected neurons with Pattern IIb (with well-developed neurofibrillary tangles) had a relatively small dendritic tree, with thin dendrites and very few or no spines, which may simply be due to a more advanced stage of atrophy. Thus, if we assume the widely accepted hypothesis that neuronal degeneration and atrophy is progressive, our observations suggest that such processes begin with synaptic disconnection of the dendritic regions distal to the soma. This progressive disconnection must be analysed in detail given the functional implication for the spatial segregation of synaptic connections implicated in the type of information transmitted. This is not only evident for the proximal, intermediate and distal dendrites of pyramidal neurons in the hippocampus, where neurons in all cornu ammonis fields establish different types of synaptic contacts in each strata that they traverse (Andersen *et al*., 2007), but it may also occur in other cortical regions. For example, the synaptic connections of axons that arise within the same cortical column in the neocortex preferentially innervate the proximal basal dendrites of pyramidal cells (Markram *et al*., 1997; Feldmeyer *et al*., 2002). Moreover, the proximal and distal segments of basal dendrites have different characteristics with respect to integration and synaptic plasticity (Markram *et al*., 1997; Hausser and Mel, 2003; Gordon *et al*., 2006; Gelfo *et al*., 2009; Branco and Häusser, 2011). These observations suggest that cellulipetal disconnection may occur and that the functional consequences of such a process are likely to be selective and progressive in the cerebral cortex as a whole, at least at the cellular level. Finally, there are some dendritic branches within a given neuron that are more affected than others, suggesting that this cellulipetal disconnection does not occur synchronously across the whole dendritic arbor.

In conclusion, neurons in the human brain that are recognized by PHF-tau$_{AT8}$ and PHF-tau$_{PHF-1}$ have not necessarily suffered severe and irreversible effects but rather, the characteristic cognitive impairment in Alzheimer's disease is likely to depend on the relative number of neurons that are in intermediate and advanced stages of a neurofibrillar pathology, among other factors.

Acknowledgements

The authors are grateful to Félix Hernández for his helpful comments on the manuscript and Lorena Valdés for her technical assistance.

Funding

This work was supported by grants from the following entities: CIBERNED (CB06/05/0066), Fundación CIEN (Financiación de Proyectos de Investigación de Enfermedad de Alzheimer y enfermedades relacionadas 2008), Fundación Caixa (BM05-47-0) and the Spanish Ministry of Economy and Competitiveness (SAF2009-09394 and BFU2012-34963). The authors declare that the research was carried out in the absence of any commercial or financial relationships that might be construed as a potential conflict of interest.

Supplementary material

Supplementary material is available at *Brain* online.

References

Alonso A, Zaidi T, Novak M, Grundke-Iqbal I, Iqbal K. Hyperphosphorylation induces self-assembly of tau into tangles of paired helical filaments/straight filaments. Proc Natl Acad Sci USA 2001; 98: 6923–8.

Alonso AD, Di Clerico J, Li B, Corbo CP, Alaniz ME, Grundke-Iqbal I, et al. Phosphorylation of tau at Thr212, Thr231, and Ser262 combined causes neurodegeneration. J Biol Chem 2010; 285: 30851–60.

Alonso Adel C, Li B, Grundke-Iqbal I, Iqbal K. Polymerization of hyperphosphorylated tau into filaments eliminates its inhibitory activity. Proc Natl Acad Sci USA 2006; 103: 8864–9.

Andersen P, Morris R, Amaral D, Bliss T, O'Keefe J, editors. The Hippocampus Book. New York: Oxford University Press; 2007.

Andorfer C, Kress Y, Espinoza M, de Silva R, Tucker KL, Barde YA, et al. Hyperphosphorylation and aggregation of tau in mice expressing normal human tau isoforms. J Neurochem 2003; 86: 582–90.

Araya R, Jiang J, Eisenthal KB, Yuste R. The spine neck filters membrane potentials. Proc Natl Acad Sci USA 2006; 103: 17961–6.

Arellano JI, Benavides-Piccione R, Defelipe J, Yuste R. Ultrastructure of dendritic spines: correlation between synaptic and spine morphologies. Front Neurosci 2007a; 1: 131–43.

Arellano JI, Espinosa A, Fairen A, Yuste R, DeFelipe J. Non-synaptic dendritic spines in neocortex. Neuroscience 2007b; 145: 464–9.

Arendt T, Stieler J, Strijkstra AM, Hut RA, Rudiger J, Van der Zee EA, et al. Reversible paired helical filament-like phosphorylation of tau is an adaptive process associated with neuronal plasticity in hibernating animals. J Neurosci 2003; 23: 6972–81.

Avila J, León-Espinosa G, García E, García-Escudero V, Hernández F, DeFelipe J. Tau phosphorylation by GSK3 in different conditions. Int J Alzheimers Dis 2012; 2012: 578373.

Avila J, Lucas JJ, Perez M, Hernandez F. Role of tau protein in both physiological and pathological conditions. Physiol Rev 2004; 84: 361–84.

Bancher C, Brunner C, Lassmann H, Budka H, Jellinger K, Wiche G, et al. Accumulation of abnormally phosphorylated tau precedes the formation of neurofibrillary tangles in Alzheimer's disease. Brain Res 1989; 477: 90–9.

Benavides-Piccione R, Ballesteros-Yáñez I, Martínez de Legrán M, Elston G, Estivill X, Fillat C, et al. On dendrites in Down syndrome and DS murine models: a spiny way to learn. Prog Neurobiol 2004; 74: 111–26.

Benavides-Piccione R, Fernaud-Espinosa I, Robles V, Yuste R, DeFelipe J. Age-based comparison of human dendritic spine structure using complete three-dimensional reconstructions. Cereb Cortex 2012. Advance Access published on June 17, 2012, doi: 10.1093/cercor/bhs154.

Bittner T, Fuhrmann M, Burgold S, Ochs SM, Hoffmann N, Mitteregger G, et al. Multiple events lead to dendritic spine loss in triple transgenic Alzheimer's disease mice. PLoS One 2010; 5: e15477.

Blazquez-Llorca L, Garcia-Marin V, Defelipe J. Pericellular innervation of neurons expressing abnormally hyperphosphorylated tau in the hippocampal formation of Alzheimer's disease patients. Front Neuroanat 2010; 4: 20.

Blazquez-Llorca L, Garcia-Marin V, Merino-Serrais P, Ávila J, DeFelipe J. Abnormal tau phosphorylation in the thorny excrescences of CA3 hippocampal neurons in patients with Alzheimer's disease. J Alzheimers Dis 2011; 26: 683–98.

Bloodgood BL, Sabatini BL. Neuronal activity regulates diffusion across the neck of dendritic spines. Science 2005; 310: 866–9.

Braak H, Braak E. Neuropathological stageing of Alzheimer-related changes. Acta Neuropathol 1991; 82: 239–59.

Braak E, Braak H, Mandelkow EM. A sequence of cytoskeleton changes related to the formation of neurofibrillary tangles and neuropil threads. Acta Neuropathol 1994; 87: 554–67.

Branco T, Häusser M. Synaptic integration gradients in single cortical pyramidal cell dendrites. Neuron 2011; 69: 885–92.

Buhl EH, Schwerdtfeger WK, Germroth P. Intracellular injection of neurons in fixed brain tissue combined with other neuroanatomical techniques at the light- and electron- microscopic level. In: Björklund A, Hökfelt T, Wouterloud FG, van den Pol AN, editors. Handbook of chemical neuroanatomy, Vol. 8: Methods for the analysis of neuronal microcircuits. Amsterdam: Elsevier; 1990. p. 273–303.

Castellani RJ, Nunomura A, Lee HG, Perry G, Smith MA. Phosphorylated tau: toxic, protective, or none of the above. J Alzheimers Dis 2008; 14: 377–83.

Cente M, Filipcik P, Pevalova M, Novak M. Expression of a truncated tau protein induces oxidative stress in a rodent model of tauopathy. Eur J Neurosci 2006; 24: 1085–90.

DeFelipe J, Fariñas I. The pyramidal neuron of the cerebral cortex: morphological and chemical characteristics of the synaptic inputs. Prog Neurobiol 1992; 39: 563–607.

Dobrunz LE, Stevens CF. Heterogeneity of release probability, facilitation, and depletion at central synapses. Neuron 1997; 18: 995–1008.

Einstein G. Intracellular injection of Lucifer yellow into cortical neurons in lightly fixed sections and its application to human autopsy material. J Neurosci Methods 1988; 26: 95–103.

Elston GN, Benavides-Piccione R, DeFelipe J. The pyramidal cell in cognition: a comparative study in human and monkey. J Neurosci 2001; 21: RC163.

Feldmeyer D, Lubke J, Silver RA, Sakmann B. Synaptic connections between layer 4 spiny neurone-layer 2/3 pyramidal cell pairs in juvenile rat barrel cortex: physiology and anatomy of interlaminar signalling within a cortical column. J Physiol 2002; 538: 803–22.

Fiala JC, Spacek J, Harris KM. Dendritic spine pathology: cause or consequence of neurological disorders? Brain Res Brain Res Rev 2002; 39: 29–54.

Garcia-Marin V, Blazquez-Llorca L, Rodriguez JR, Boluda S, Muntane G, Ferrer I, et al. Diminished perisomatic GABAergic terminals on cortical neurons adjacent to amyloid plaques. Front Neuroanat 2009; 3: 28.

Gelfo F, De Bartolo P, Giovine A, Petrosini L, Leggio MG. Layer and regional effects of environmental enrichment on the pyramidal neuron morphology of the rat. Neurobiol Learn Mem 2009; 91: 353–65.

Gordon U, Polsky A, Schiller J. Plasticity compartments in basal dendrites of neocortical pyramidal neurons. J Neurosci 2006; 26: 12717–26.

Grundke-Iqbal I, Iqbal K, Tung YC, Quinlan M, Wisniewski HM, Binder LI. Abnormal phosphorylation of the microtubule-associated protein tau (tau) in Alzheimer cytoskeletal pathology. Proc Natl Acad Sci USA 1986; 83: 4913–17.

Hanger DP, Anderton BH, Noble W. Tau phosphorylation: the therapeutic challenge for neurodegenerative disease. Trends Mol Med 2009; 15: 112–19.

Harris KM, Stevens JK. Dendritic spines of CA 1 pyramidal cells in the rat hippocampus: serial electron microscopy with reference to their biophysical characteristics. J Neurosci 1989; 9: 2982–97.

Hausser M, Mel B. Dendrites: bug or feature? Curr Opin Neurobiol 2003; 13: 372–83.

Heffernan JM, Eastwood SL, Nagy Z, Sanders MW, McDonald B, Harrison PJ. Temporal cortex synaptophysin mRNA is reduced in Alzheimer's disease and is negatively correlated with the severity of dementia. Exp Neurol 1998; 150: 235–9.

Holmes WR. The role of dendritic diameters in maximizing the effectiveness of synaptic inputs. Brain Res 1989; 478: 127–37.

Honer WG, Dickson DW, Gleeson J, Davies P. Regional synaptic pathology in Alzheimer's disease. Neurobiol Aging 1992; 13: 375–82.

Iqbal K, Alonso Adel C, Chen S, Chohan MO, El-Akkad E, Gong CX, et al. Tau pathology in Alzheimer disease and other tauopathies. Biochim Biophys Acta 2005; 1739: 198–210.

Iqbal K, Liu F, Gong CX, Alonso Adel C, Grundke-Iqbal I. Mechanisms of tau-induced neurodegeneration. Acta Neuropathol 2009; 118: 53–69.

Jacobs B, Schall M, Prather M, Kapler L, Driscoll L, Baca S, et al. Regional dendritic and spine variation in human cerebral cortex: a quantitative study. Cereb Cortex 2001; 11: 558–71.

Knafo S, Alonso-Nanclares L, Gonzalez-Soriano J, Merino-Serrais P, Fernaud-Espinosa I, Ferrer I, et al. Widespread changes in dendritic spines in a model of Alzheimer's disease. Cereb Cortex 2009a; 19: 586–92.

Knafo S, Venero C, Merino-Serrais P, Fernaud-Espinosa I, Gonzalez-Soriano J, Ferrer I, et al. Morphological alterations to neurons of the amygdala and impaired fear conditioning in a transgenic mouse model of Alzheimer's disease. J Pathol 2009b; 219: 41–51.

Lee HG, Perry G, Moreira PI, Garrett MR, Liu Q, Zhu X, et al. Tau phosphorylation in Alzheimer's disease: pathogen or protector? Trends Mol Med 2005; 11: 164–9.

Li B, Yamamori H, Tatebayashi Y, Shafit-Zagardo B, Tanimukai H, Chen S, et al. Failure of neuronal maturation in Alzheimer disease dentate gyrus. J Neuropathol Exp Neurol 2008; 67: 78–84.

Lue LF, Brachova L, Civin WH, Rogers J. Inflammation, A beta deposition, and neurofibrillary tangle formation as correlates of Alzheimer's disease neurodegeneration. J Neuropathol Exp Neurol 1996; 55: 1083–8.

Luebke JI, Weaver CM, Rocher AB, Rodriguez A, Crimins JL, Dickstein DL, et al. Dendritic vulnerability in neurodegenerative disease: insights from analyses of cortical pyramidal neurons in transgenic mouse models. Brain Struct Funct 2010; 214: 181–99.

Mainen ZF, Sejnowski TJ. Influence of dendritic structure on firing pattern in model neocortical neurons. Nature 1996; 382: 363–6.

Majewska A, Brown E, Ross J, Yuste R. Mechanisms of calcium decay kinetics in hippocampal spines: role of spine calcium pumps and calcium diffusion through the spine neck in biochemical compartmentalization. J Neurosci 2000a; 20: 1722–34.

Majewska A, Tashiro A, Yuste R. Regulation of spine calcium compartmentalization by rapid spine motility. J Neurosci 2000b; 20: 8262–8268.

Markram H, Lubke J, Frotscher M, Roth A, Sakmann B. Physiology and anatomy of synaptic connections between thick tufted pyramidal neurones in the developing rat neocortex. J Physiol 1997; 500: 409–40.

Masliah E, Ellisman M, Carragher B, Mallory M, Young S, Hansen L, et al. Three-dimensional analysis of the relationship between synaptic pathology and neuropil threads in Alzheimer disease. J Neuropathol Exp Neurol 1992; 51: 404–14.

Merino-Serrais P, Knafo S, Alonso-Nanclares L, Fernaud-Espinosa I, DeFelipe J. Layer-specific alterations to CA1 dendritic spines in a mouse model of Alzheimer's disease. Hippocampus 2011; 21: 1037–44.

Mirra SS, Heyman A, McKeel D, Sumi SM, Crain BJ, Brownlee LM, et al. The Consortium to Establish a Registry for Alzheimer's Disease (CERAD). Part II. Standardization of the neuropathologic assessment of Alzheimer's disease. Neurology 1991; 41: 479–86.

Mocanu MM, Nissen A, Eckermann K, Khlistunova I, Biernat J, Drexler D, et al. The potential for beta-structure in the repeat domain of tau protein determines aggregation, synaptic decay, neuronal loss, and coassembly with endogenous Tau in inducible mouse models of tauopathy. J. Neurosci 2008; 28: 737–48.

Mohorko N, Repovs G, Popović M, Kovacs GG, Bresjanac M. Curcumin labeling of neuronal fibrillar tau inclusions in human brain samples. J Neuropathol Exp Neurol 2010; 69: 405–14.

Nusser Z, Lujan R, Laube G, Roberts JD, Molnar E, Somogyi P. Cell type and pathway dependence of synaptic AMPA receptor number and variability in the hippocampus. Neuron 1998; 21: 545–59.

Penzes P, Cahill ME, Jones KA, VanLeeuwen JE, Woolfrey KM. Dendritic spine pathology in neuropsychiatric disorders. Nat Neurosci 2011; 14: 285–93.

Popov VB, Bocharova LS. Hibernation-induced structural changes in synaptic contacts between mossy fibre and hippocampal pyramidal neurons. Neuroscience 1992; 48: 53–62.

Price JL, McKeel DW Jr, Buckles VD, Roe CM, Xiong C, Grundman M, et al. Neuropathology of nondemented aging: presumptive evidence for preclinical Alzheimer disease. Neurobiol Aging 2009; 30: 1026–36.

Rocher AB, Crimins JL, Amatrudo JM, Kinson MS, Todd-Brown MA, Lewis J, et al. Structural and functional changes in tau mutant mice neurons are not linked to the presence of NFTs. Exp Neurol 2010; 223: 385–93.

Samuel W, Alford M, Hofstetter CR, Hansen L. Dementia with Lewy bodies versus pure Alzheimer disease: differences in cognition, neuropathology, cholinergic dysfunction, and synapse density. J Neuropathol Exp Neurol 1997; 56: 499–508.

Santacruz K, Lewis J, Spires T, Paulson J, Kotilinek L, Ingelsson M, et al. Tau suppression in a neurodegenerative mouse model improves memory function. Science 2005; 309: 476–81.

Santa-María I, Pérez M, Hernández F, Avila J, Moreno FJ. Characteristics of the binding of thioflavin S to tau paired helical filaments. J Alzheimers Dis 2006; 9: 279–85.

Schikorski T, Stevens C. Quantitative fine-structural analysis of olfactory cortical synapses. Proc Natl Acad Sci USA 1999; 96: 4107–12.

Schikorski T, Stevens CF. Quantitative ultrastructural analysis of hippocampal excitatory synapses. J Neurosci 1997; 17: 5858–67.

Schikorski T, Stevens CF. Morphological correlates of functionally defined synaptic vesicle populations. Nat Neurosci 2001; 4: 391–5.

Smith KD, Kallhoff V, Zheng H, Pautler RG. In vivo axonal transport rates decrease in a mouse model of Alzheimer's disease. Neuroimage 2007; 35: 1401–8.

Spires TL, Meyer-Luehmann M, Stern EA, McLean PJ, Skoch J, Nguyen PT, et al. Dendritic spine abnormalities in amyloid precursor protein transgenic mice demonstrated by gene transfer and intravital multiphoton microscopy. J Neurosci 2005; 25: 7278–87.

Spires-Jones T, Knafo S. Spines, plasticity, and cognition in Alzheimer's model mice. Neural Plast 2012; 2012: 1–10.

Spires-Jones TL, de Calignon A, Matsui T, Zehr C, Pitstick R, Wu HY, et al. In vivo imaging reveals dissociation between caspase activation and acute neuronal death in tangle-bearing neurons. J Neurosci 2008; 28: 862–7.

Spruston N. Pyramidal neurons: dendritic structure and synaptic integration. Nat Rev Neurosci 2008; 9: 206–21.

Stamer K, Vogel R, Thies E, Mandelkow E, Mandelkow EM. Tau blocks traffic of organelles, neurofilaments, and APP vesicles in neurons and enhances oxidative stress. J Cell Biol 2002; 156: 1051–63.

Terry RD, Masliah E, Salmon DP, Butters N, DeTeresa R, Hill R, et al. Physical basis of cognitive alterations in Alzheimer's disease: synapse loss is the major correlate of cognitive impairment. Ann Neurol 1991; 30: 572–80.

Terwel D, Dewachter I, Van Leuven F. Axonal transport, tau protein, and neurodegeneration in Alzheimer's disease. Neuromolecular Med 2002; 2: 151–65.

Toni N, Laplagne DA, Zhao C, Lombardi G, Ribak CE, Gage FH, et al. Neurons born in the adult dentate gyrus form functional synapses with target cells. Nat Neurosci 2008; 11: 901–7.

Tsai J, Grutzendler J, Duff K, Gan WB. Fibrillar amyloid deposition leads to local synaptic abnormalities and breakage of neuronal branches. Nat Neurosci 2004; 7: 1181–3.

Vetter P, Roth A, Hausser M. Propagation of action potentials in dendrites depends on dendritic morphology. J Neurophysiol 2001; 85: 926–37.

Wakabayashi K, Honer WG, Masliah E. Synapse alterations in the hippocampal-entorhinal formation in Alzheimer's disease with and without Lewy body disease. Brain Res 1994; 667: 24–32.

Wang JZ, Grundke-Iqbal I, Iqbal K. Kinases and phosphatases and tau sites involved in Alzheimer neurofibrillary degeneration. Eur J Neurosci 2007; 25: 59–68.

Wang JZ, Liu F. Microtubule-associated protein tau in development, degeneration and protection of neurons. Prog Neurobiol 2008; 85: 148–75.

Yuste R. Dendritic spines. Cambridge, MA: MIT Press; 2010.

Yuste R, Majewska A, Holthoff K. From form to function: calcium compartmentalization in dendritic spines. Nat Neurosci 2000; 3: 653–9.